Contents lists available at SciVerse ScienceDirect

Optics Communications

journal homepage: www.elsevier.com/locate/optcom

Discussion

Monolithic silicon-based 16-QAM modulator using two plasmonic phase shifters

Fei Li, Mu Xu, Xiaofeng Hu, Jiayang Wu, Tao Wang, Yikai Su*

State Key Lab of Advanced Optical Communication Systems and Networks, Department of Electronic Engineering, Shanghai Jiao Tong University, Shanghai 200240, China

ABSTRACT

We propose a compact silicon-based modulator for 16-point quadrature amplitude modulation (16-QAM) with a simple structure using two phase shifters. The phase shifters employ low-loss hybrid plasmon waveguide, consisting of a conductor-gap-dielectric structure filled with polymer. Combining the strong optical confinement ability of the plasmonic waveguide with the highly nonlinear characteristic of the polymer, the proposed 16-QAM modulator can achieve a compact footprint, high-speed operation, and low power consumption, potentially allowing for high-density on-chip integration and broadband long-haul optical transmission.

© 2012 Elsevier B.V. All rights reserved.

1. Introduction

Advanced modulation formats such as quadrature amplitude modulation (QAM) have attracted much attention due to their capability to improve spectral efficiency in long-haul optical transmission. Integrated optical devices for QAM modulation are desirable for high-performance and cost-effective QAM systems. Monolithically integrated 16-QAM modulators have been demonstrated with $LiNbO_3$ Mach–Zehnder modulators (MZMs) [1,2], group III–V modulators [3,4], and silicon microring modulators [5]. However, $LiNbO_3$ MZMs and group III–V modulators occupy large footprints on the scale of centimeters [6] and millimeters [3], respectively. Recent breakthroughs in silicon-based optical modulators make silicon photonics a promising platform for next-generation photonic integrated circuits (PICs), owing to their compact size, compatibility with existing CMOS microelectronic technology, and potentially low power consumption. Among them, silicon microring modulators relying on free carrier dispersion have small ring radii of a few micrometers [5], but the achievable modulation bandwidth is limited by time constants related to the injection or removal of free carriers from the modulation arm [7]. In contrast, silicon-organic hybrid (SOH) modulators allow for high-bandwidth modulation [8–10] because electro-optic (EO) polymers can offer very high Pockels coefficient

$(r_{33} > 300\ pm/V)$ and fast response speed extending up to the terahertz frequency range [11]. However, the relatively large portion of energy distributed in the silicon regions may result in a relatively small overlap between the active material and the optical mode, thus lowering the modulation efficiency of such modulators [12]. The structure size, the drive voltage, and the electrical power dissipation can be further reduced by employing more compact waveguides.

Alternatively, surface plasmon polaritons (SPPs), which propagate along metal–dielectric interfaces, have been utilized as an effective approach to overcome the diffraction limit that exists in conventional photonic technology, thus guiding and confining light at the deep sub-wavelength scale [13]. Such strong confinement thereby enhances the interaction with the underlying material and hence the modulation of the optical signal. Several approaches have been proposed to electrically modulate the intensity [13–17] or phase [18] of the SPPs. Among them, polymer-plasmonic waveguide based modulators [13,14,18] can combine highly nonlinear characteristics of polymers with strong optical confinement abilities of plasmonic waveguides, achieving ultrahigh-speed operation with an ultra-compact footprint. Sun et al. proposed a phase modulator based on a horizontal metal–polymer–silicon–polymer–metal waveguide [18]. However, its propagation loss is as high as 0.828 dB/μm, resulting in a high insertion loss. This design also needs to deposit polymer non-uniformly, which is challenging.

In this letter, we propose a compact silicon-based 16-QAM modulator using a simple structure with two plasmonic phase

* Corresponding author. Tel.: +86 021 34204425; fax: +86 021 34204370.
E-mail address: yikaisu@sjtu.edu.cn (Y. Su).

shifters. Normally, plasmonic phase modulators suffer from a high propagation loss [18]. Here, we design a low-loss phase shifter incorporating a hybrid plasmon waveguide consisting of a conductor-gap-dielectric structure filled with polymer [19]. By taking advantage of the intrinsic loss in the plasmonic phase shifter to form different amplitudes of signals required for QAM signal generation, the proposed 16-QAM modulator has a simple configuration, a small footprint of less than 100 μm, and a moderate insertion loss of about 5.17 dB. The phase shifter has a low voltage–length product $V_\pi L$ of only 0.07 Vmm, a potentially ultrahigh modulation bandwidth, and a low propagation loss of 0.078 dB/μm at 1550-nm wavelength, making it suitable for on-chip integration. To the best of our knowledge, this is the first proposal to generate a 16-QAM signal using plasmonic phase shifters.

2. Monolithic 16-QAM modulator structure

The schematic of the proposed 16-QAM modulator is shown in Fig. 1. Silicon on insulator (SOI) structure is assumed. Input and output waveguides are conventional silicon strip waveguides, with width and height set to be 400 and 250 nm, respectively. A Y-splitter distributes the power equally into two arms. A phase shifter driven with a 4-level data$_1$ is employed in the upper arm to generate a quadrature phase shift keying (QPSK) signal, while the light in the lower arm remains un-modulated. An offset 4-QAM signal is synthesized with a Y-combiner by recombining the two arms with a 6-dB intensity difference. A DC bias can be applied to the first phase shifter to accurately adjust the phase difference between the upper and lower arms. By employing another phase shifter driven with a 4-level data$_2$, a square 16-QAM signal is obtained and 16 symbols are mapped with equal spacing. For a more practical design, the Y-splitter and Y-combiner could be replaced by multi-mode interference (MMI) couplers. We utilize commercial software VPI TransmissionMaker[6.5] to generate the 16-QAM signal and MATLAB software to process data. The inset in Fig. 1 depicts the back-to-back constellation diagram for the square 16-QAM signal.

In the previous 16-QAM generation schemes, four [3,4] or even eight [1,2] phase modulators and four electro-absorption modulators (EAMs) [3] with more than four electrodes were needed, making the structure complex and the bias control complicated. Accurate power splitting in these schemes [3,4] is also challenging. In contrast, our 16-QAM modulator has a very simple and compact configuration with only two phase shifters and requires one DC bias, leading to a much smaller footprint, lower power consumption and easier bias control, though at the expense of relatively high accuracy of the modulation voltages.
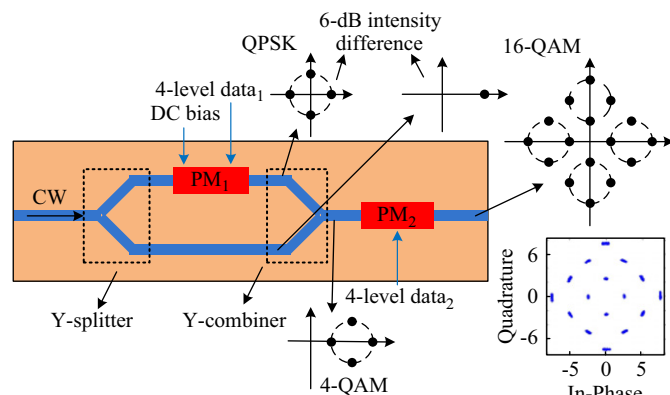
It should be noted that plasmonic–organic phase shifters are advantageous over SOH counterparts in that plasmonic phase shifters can achieve stronger optical confinement and therefore higher modulation efficiency and much shorter length than SOH counterparts. They also eliminate the need for a traveling wave structure. Moreover, one can take advantage of the intrinsic propagation loss in the plasmonic phase shifter to form the 6-dB intensity difference without introducing any additional attenuators, thus greatly simplifying the design of the 16-QAM modulator and fabrication process.

3. The hybrid plasmonic phase shifter

3.1. Device structure and analysis

Fig. 2(a) shows the schematic perspective view of the proposed plasmonic phase shifter used in the 16-QAM modulator, connected with silicon strip waveguides. The cross-sectional view of the phase shifter is shown in Fig. 2(b), consisting of a 25 wt% $C_{32}H_{28}F_3N_4O$-doped Poly(methyl methacrylate) (PMMA) active core sandwiched between silver (Ag) and silicon layers in the perpendicular direction. The optical field is confined in the nanoscale polymer slot, and can be clearly seen in the inset of Fig. 2, where the amplitude of the dominant electric field $E_y(x, y)$ distribution for the fundamental transverse magnetic (TM) mode at 1550-nm wavelength is plotted. The coordinate systems are also depicted in Fig. 2. The center of the silicon rib defines the origin ($x=y=0$). The mode is obtained by using the finite element method (FEM) based commercial software COMSOL Multiphysics3.5a. The corresponding refractive indices at 1550 nm for Si, SiO$_2$ and PMMA are set to be 3.48, 1.45 and 1.635 [20], respectively. The permittivity of silver is set to be $-133.75+3.337i$ [21]. The silicon rib and strip marked as n− silicon and n+ silicon in Fig. 2(b), respectively, are doped with phosphorus to serve as electrical conductors from the metallic contact pads. The doping concentrations are approximately 10^{18} cm^{-3} and 10^{20} cm^{-3}, respectively. A conservative 5-μm metal-to-waveguide clearance is used to locate the side metal electrodes outside the optical modal field to avoid excess losses and to ease alignment tolerances [22]. The imaginary parts of the refractive indices of the silicon rib and strip induced by implant are estimated to be 0.0000185 and 0.0037, respectively [23]. The two top silica strips
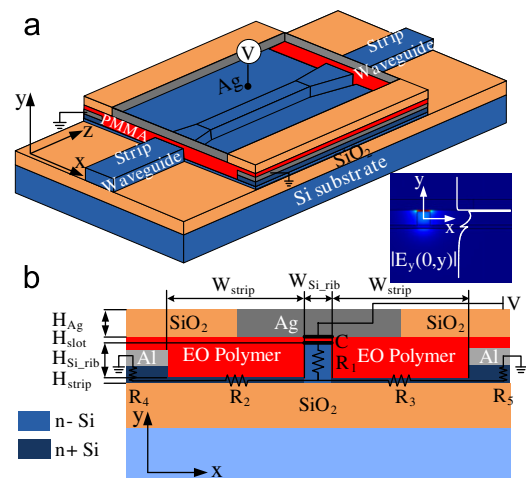

Fig. 1. The schematic of the 16-QAM modulator. The inset is the simulated back-to-back square 16-QAM constellation.

Fig. 2. Schematic perspective view (a), the cross section and equivalent circuit (b), of the proposed plasmonic phase shifter connected with silicon strip waveguides. The inset shows the calculated field distribution for the amplitude of the major component $E_y(x,y)$ of the fundamental TM mode at 1550 nm.
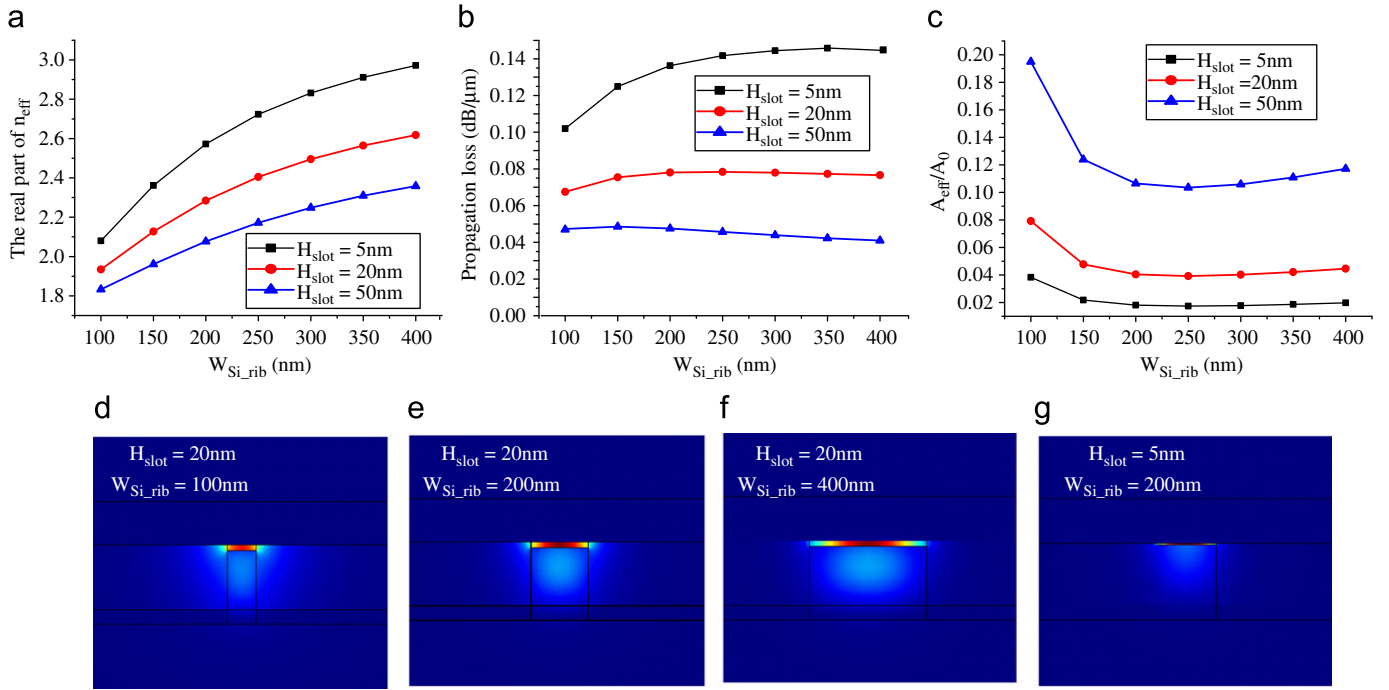
Fig. 3. For the cases of $H_{slot} = 5$, 20, and 50 nm, the real part of the effective refractive index n_{eff} (a), the propagation loss (b), and normalized mode area (c) as silicon rib width W_{Si_rib} varies. (d–g) Electromagnetic energy density distributions for different silicon rib width and slot height while other structural parameters are kept the same.

eliminate undesired capacitance formed between the top Ag electrode and the two side aluminum (Al) electrodes.

The total height of the silicon rib and silicon strip is set to 250 nm to remain consistent with the height of silicon strip waveguide. To achieve high-bandwidth modulation, low-resistance silicon rib and strip should be made to avoid a large RC time constant. The thicker strip naturally decreases the resistance in accordance with Ohm's law, but complicates the waveguide design process [24]. In this case we choose the height of the strip, H_{strip}, to be 50 nm as a trade-off between resistance and fabrication challenge, thus the height of the silicon rib, H_{Si_rib}, is 200 nm. The thickness of the Ag layer is fixed at 150 nm. Its impact on phase shift will be discussed in Section 3.2. In the following study, we vary the silicon rib width, W_{Si_rib}, and the slot height, H_{slot}, to control the effective refractive index, propagation loss, and effective mode area, A_{eff}, at 1550-nm wavelength.

Fig. 3(a–c) show the real part of the effective refractive index, propagation loss and normalized mode area (A_{eff}/A_0), respectively, of the hybrid plasmonic waveguide for various H_{slot} and W_{Si_rib} settings. The propagation loss is given by $2k_0 n_{im} 10 lg(e)$, where k_0 is the free space wave-number, n_{im} is the imaginary part of the effective refractive index, and $10 lg(e) = 4.34$. The effective mode area, A_{eff}, is calculated using $(\iint |E|^2 dxdy)^2/(\iint |E|^4 dxdy)$. A_0 is the diffraction-limited mode area and defined as $\lambda^2/4$. For a given W_{Si_rib}, the real part of the effective index and propagation loss both tend to increase as slot thickness decreases since the mode is strongly confined within the slot, as shown in Fig. 3(e) and (g), thus leading to smaller mode area. When H_{slot} is fixed, as W_{Si_rib} is reduced, there is more electromagnetic energy distributed over the side polymer and less energy confined in the slot than those of a relatively larger W_{Si_rib} as shown in Fig. 3(d) and (e), resulting in smaller real part of the effective refractive index, lower propagation loss, and larger normalized mode area. As W_{Si_rib} continues to increase, there is more optical field confined in the silicon rib as depicted in Fig. 3(f), so the mode area starts to increase. For the same reason, the real part of the effective refractive index increases as the propagation loss goes down.

3.2. Phase modulation and device optimization

Device parameters, including slot height and silicon rib width, are optimized in order to maximize the amount of shift in effective index as a function of applied voltage. We use the Pockels effect of the EO polymer to achieve phase shift. The polymer refractive index change $\Delta n_{polymer}$ with respect to external voltage U between the top and side metal electrodes is given by [25]:

$$\Delta n_{polymer} = -r_{33} n_{polymer}^3 U/(2H_{slot}) \qquad (1)$$

where r_{33} and $n_{polymer}$ are the Pockels coefficient and intrinsic refractive index of the polymer, respectively. In this case, r_{33} of the polymer is 150 pm/V [26]. The change in the index of the polymer $\Delta n_{polymer}$ gives rise to a change in the effective refractive index Δn_{eff} and results in a phase shift:

$$\Delta\phi = 2\pi \Delta n_{eff,re} L/\lambda \qquad (2)$$

in the waveguide, where L is the length of the hybrid plasmonic phase shifter and λ is the wavelength of light in free space. Δn_{eff} is calculated using commercial software COMSOL Multiphysics3.5a.

Fig. 4(a) shows the dependence of $\Delta n_{eff,re}$ on W_{Si_rib} and H_{slot} with an external voltage of $U = 0.5$V. $\Delta n_{eff,re}$ increases with the decrease of W_{Si_rib} at a given H_{slot} due to a stronger overlap between the polymer and the optical field, which is consistent with the analysis above. A smaller slot thickness leads to a larger effective refractive index change and consequently a larger phase shift, as can be easily derived from Eqs. (1) and (2). From Fig. 4(a), one can see that in order to achieve the maximum phase shift, a small W_{Si_rib} and H_{slot} are expected. However, there are practical limitations such as fabrication restrictions and dielectric breakdown of the polymer under excessive field strengths. The breakdown field in the EO polymer is typically approximately 3 MV/cm [27,28], such that for a 5-nm slot a maximum drive voltage of only 1.5 V is needed. The length of the phase shifter must be long enough to achieve a low drive voltage, resulting in high propagation loss. Consequently, the height of the slot is set to be 20 nm to make a trade-off between
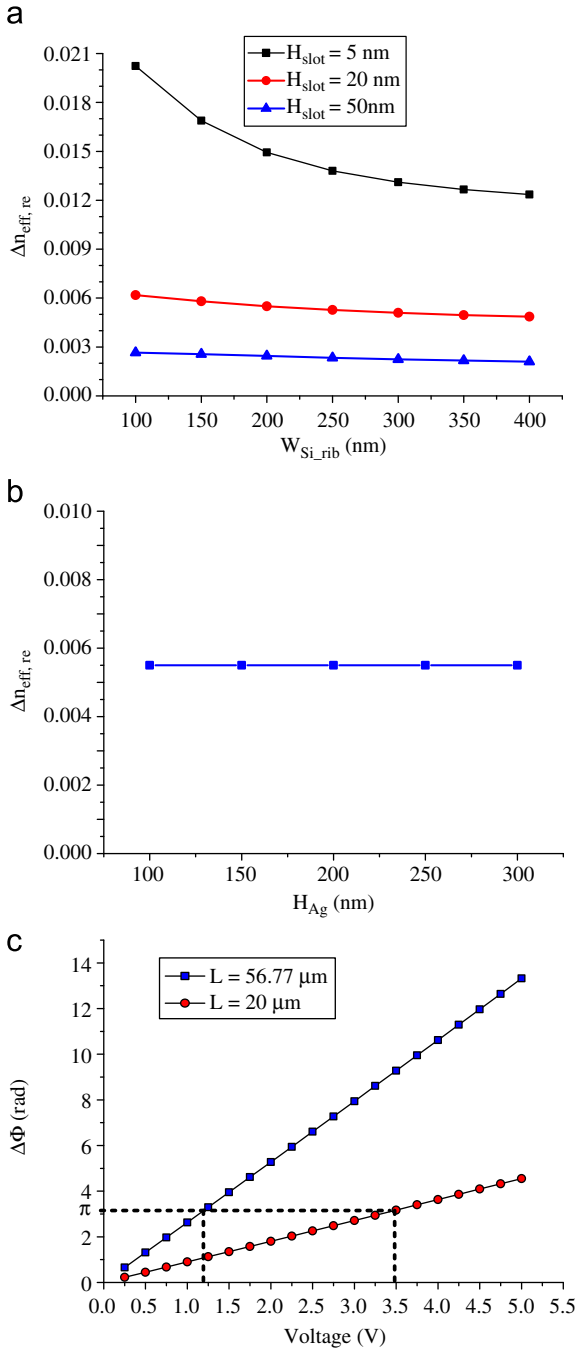
Fig. 4. The real part of the effective refractive index changes $\Delta n_{eff,re}$ versus silicon rib width W_{Si_rib} (a) and Ag layer thickness H_{Ag} (b), respectively, with an applied voltage of 0.5 V. (c) The phase shift curves for the 56.77-µm-long and 20-µm-long phase shifters.

modulation efficiency and propagation loss. The silicon rib width is chosen as 200 nm to balance the modulation effect and mode area. We then analyze the effective index change as a function of Ag layer thickness, as depicted in Fig. 4(b). We find that $\Delta n_{eff,re}$ does not change much as the Ag thickness varies, which relaxes the demand for accurate metal thickness control. Thus, the optimal structural dimensions are chosen as $W_{Si\_rib} = 200$ nm, $H_{Si\_rib} = 200$ nm, $W_{strip} = 5$ µm, $H_{strip} = 50$ nm, $H_{slot} = 20$ nm, and $H_{Ag} = 150$ nm. The propagation loss of this specific device is 0.078 dB/µm at 1550 nm, as shown in Fig. 3(b); this is much lower than the plasmonic phase modulator in [18].

Once all the structural parameters of the phase shifter have been chosen, one can calculate the length of the first phase shifter needed to form the 6-dB intensity difference in the 16-QAM modulator. There are two factors to be taken into consideration, the coupling loss between the silicon strip waveguide and the phase shifter, and the propagation loss of the phase shifter. To effectively couple light into the 20-nm slot region from the silicon strip waveguide, a 500-nm-long plasmonic taper [29] is employed to minimize the group index mismatch between the two types of waveguides. In order to improve the coupling efficiency and simplify the fabrication process, the Ag layer and slot are not tapered in our design, as can be seen in Fig. 2(a). The coupling efficiency can reach as high as 83.44%, corresponding to a coupling loss of 0.786 dB/facet, calculated by commercial software Lumerical FDTD solutions 7.5.3. Here we use a strip waveguide fundamental TM mode at 1550-nm wavelength as the launch field, since the waves in the plasmonic phase shifter can only be excited for the TM polarization. The length of the first phase shifter is chosen as 56.77 µm to obtain a propagation loss of ~4.428 dB considering the total coupling loss of 1.572 dB. The length of the second phase shifter is set to be 20 µm to balance the propagation loss and phase modulation efficiency. A variable-ratio power splitter [30] can be employed to replace the Y-splitter in Fig. 1 and thus accurately control the 6-dB intensity difference in case of fabrication error. The total insertion loss of our 16-QAM modulator is ~5.17 dB and the chip size is less than 100 µm.

Fig. 4(c) depicts the phase shift curves as a function of the drive voltage for the 56.77-µm and 20-µm long phase shifters, respectively. The half-wave voltages or V_π of the two phase shifters are as low as 1.2 and 3.5 V, respectively, which are both below the breakdown voltage of the polymer, as the maximum drive voltage for a 20-nm slot is 6 V.

3.3. Modulation bandwidth and power consumption

As the polymer has a very high resistivity of 10^{12} Ω cm [31], the slot together with the silicon and silver layers as the two capacitor plates, naturally form a capacitor. The equivalent circuit is drawn in Fig. 2(b). The capacitance is estimated to be 13.31 fF for the 56.77-µm-long phase shifter, calculated by $C = \varepsilon_0 \varepsilon_r A/d$, where ε_0 is the permittivity of vacuum, ε_r is the relative dielectric constant of the polymer with the value of 2.65 [32], A and d are the lateral area and thickness of the polymer in the slot, respectively. The doped silicon rib and strip have low resistivities of 2×10^{-2} Ω cm and 6×10^{-4} Ω cm [33], respectively. The calculated total resistance R is 9.7 Ω, according to Ohm's law. Therefore, the RC time constant is about 0.13 ps. As the modulation bandwidth is proportional to 1/(RC), we expect an inherent RC-limited modulation bandwidth on the order of terahertz. The bandwidth reduces in practice due to the impedance of the driver, surface states created in the course of processing silicon, and parasitic resistance in the metal pad contacts [24]. At 1.2-V and 3.5-V applied voltages for the 56.77-µm-long and 20-µm-long phase shifters, the projected power consumption is on the order of 10 fJ/bit, estimated by $P = 0.5 \, fCV_\pi^2$ [14], suitable for on-chip communication and signal processing.

3.4. Fabrication feasibility

The proposed phase shifter could be realized by using existing fabrication technologies. Here we provide a possible fabrication process depicted in Fig. 5. The device is assumed to be fabricated in a silicon-on-insulator (SOI) wafer. The silicon layer is first patterned by electron-beam lithography (EBL) followed by reactive ion etching. The silicon rib and strip are subsequently n-type doped by ion implantation to approximately 10^{18} cm^{-3}. Then the
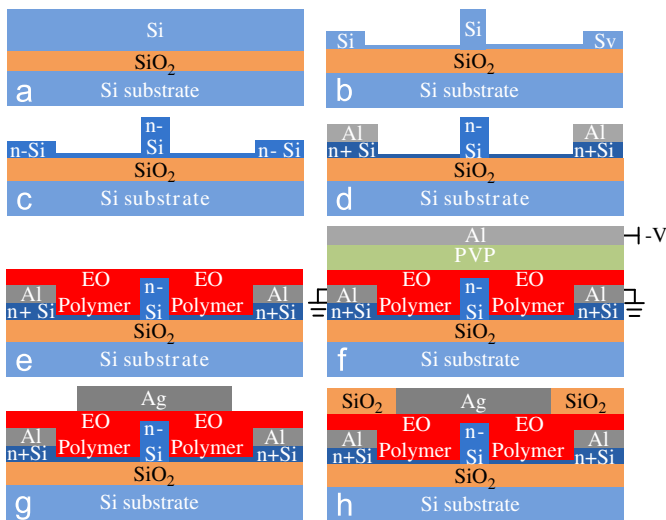
Fig. 5. The proposed fabrication process.

strip is re-doped to a total doping concentration of 10^{20} cm^{-3}, while the silicon rib is protected by photoresist from re-doping. Next, before spin-coating the EO polymer, the side metal electrodes are obtained by depositing a thin layer of Al using electron-beam evaporation and patterning it by lift-off. A layer of polyvinyl pyrrolidone (PVP) as a protective agent is deposited before depositing the top Al electrode. The polymer should be properly poled, which requires a large field intensity (>100 V/μm) to be applied between the upper metal electrode and the side metal electrodes. After removing the top metal and PVP layer, a thin layer of Ag is deposited and patterned on top to act as the upper electrode and at the same time to obtain plasmonic surface confinement. Finally, the two top silica strips are obtained with the plasma enhanced chemical vapor deposition (PECVD) technology, electron-beam lithography and reactive ion etching.

4. Conclusion

In conclusion, we have proposed a monolithic 16-QAM modulator based on two low-loss plasmonic phase shifters. The whole structure has a compact device size of less than 100 μm, an inherently large modulation bandwidth on the order of terahertz, and a moderate insertion loss of $\sim$5.17 dB. The proposed 16-QAM modulator can be integrated with other silicon-based devices to achieve high-density PICs for future communication systems.

Acknowledgments

References

[1] T. Sakamoto, A. Chiba, T. Kawanishi, Proceedings of the 33th European Conference on Optical Communication, 2007, paper PD 2.8.
[2] G.-W. Lu, T. Sakamoto, A. Chiba, T. Kawanishi, T. Miyazaki, K. Higuma, M. Sudo, J. Ichikawa, Proceedings of the 36th European Conference on Optical Communication, 2010, paper Mo.1.F.3.
[3] C.R. Doerr, P.J. Winzer, L. Zhang, L.L. Buhl, N.J. Sauer, Proceedings of the Optical Fiber Communication Conference, 2008, paper PDP20.
[4] C.R. Doerr, L. Zhang, P.J. Winzer, A.H. Gnauck, Proceedings of the Optical Fiber Communication Conference, 2011, paper OMU2.
[5] W. Jiang, Z. Shi, Proceedings of the Conference on Lasers and Electro-Optics, 2009, paper JTuD92.
[6] E.L. Wooten, K.M. Kissa, A. Yi-Yan, E.J. Murphy, D.A. Lafaw, P.F. Hallemeier, D. Maack, D.V. Attanasio, D.J. Fritz, G.J. McBrien, D.E. Bossi, IEEE Journal of Selected Topics in Quantum Electronics 6 (2000) 69.
[7] J.H. Wülbern, J. Hampe, A. Petrov, M. Eich, J. Luo, A.K.-Y. Jen, A. Di Falco, T.F. Krauss, J. Bruns, Applied Physics Letters 94 (2009) 241107.
[8] L. Alloatti, D. Korn, R. Palmer, D. Hillerkuss, J. Li, A. Barklund, R. Dinu, J. Wieland, M. Fournier, J. Fedeli, H. Yu, W. Bogaerts, P. Dumon, R. Baets, C. Koos, W. Freude, J. Leuthold, Optics Express 19 (2011) 11841.
[9] M. Hochberg, T. Baehr-Jones, G. Wang, M. Shearn, K. Harvard, J. Luo, B. Chen, Z. Shi, P. Lawson, P. Sullivan, A.K.Y. Jen, L. Dalton, A. Scherer, Nature Materials 5 (2006) 703.
[10] J.-M. Brosi, C. Koos, L.C. Andreani, M. Waldow, J. Leuthold, W. Freude, Optics Express 16 (2008) 4177.
[11] C.-Y. Lin, X. Wang, S. Chakravarty, B.S. Lee, W. Lai, J. Luo, A.K.-Y. Jen, R.T. Chen, Applied Physics Letters 97 (2010) 093304.
[12] R.F. Oulton, V.J. Sorger, D.A. Genov, D.F.P. Pile, X. Zhang, Nature Photonics 2 (2008) 496.
[13] S.-I. Inoue, S. Yokoyama, Electronics Letters 45 (2009) 1087.
[14] W. Cai, J.S. White, M.L. Brongersma, Nano Letters 9 (2009) 4403.
[15] A. Melikyan, T. Vallaitis, N. Lindenmann, T. Schimmel, W. Freude, J. Leuthold, Proceedings of the Conference on Lasers and Electro-Optics, 2010, paper JThE77.
[16] A. Melikyan, N. Lindenmann, S. Walheim, P.M. Leufke, S. Ulrich, J. Ye, P. Vincze, H. Hahn, Th. Schimmel, C. Koos, W. Freude, J. Leuthold, Optics Express 19 (2011) 8855.
[17] V.J. Sorger, N.D. Lanzillotti-Kimura, R.-M. Ma, X. Zhang, Proceedings of the Conference on Lasers and Electro-Optics, 2012, paper CTh5D.1.
[18] X. Sun, L. Zhou, X. Li, Z. Hong, J. Chen, Applied Optics 50 (2011) 3428.
[19] G. Zhou, T. Wang, P. Cao, H. Xie, F. Liu, Y. Su, Proceedings of the International Conference on Group IV Photonics, 2010, paper P1.2.
[20] H.M. Zidan, M. Abu-Elnader, Physica B: Condensed Matter 355 (2005) 308.
[21] P.B. Johnson, R.W. Christy, Physical Review B 6 (1972) 4370.
[22] M. Gould, T. Baehr-Jones, R. Ding, S. Huang, J. Luo, A.K.-Y. Jen, J.-M. Fedeli, M. Fournier, M. Hochberg, Optics Express 19 (2011) 3952.
[23] R.A. Soref, B.R. Bennett, IEEE Journal of Quantum Electronics QE-23 (1987) 123.
[24] R. Ding, T. Baehr-Jones, Y. Liu, R. Bojko, J. Witzens, S. Huang, J. Luo, S. Benight, P. Sullivan, J.-M. Fedeli, M. Fournier, L. Dalton, A. Jen, M. Hochberg, Optics Express 18 (2010) 15618.
[25] B.A. Block, T.R. Younkin, P.S. Davids, M.R. Reshotko, P. Chang, B.M. Polishak, S. Huang, J. Luo, A.K.Y. Jen, Optics Express 16 (2008) 18326.
[26] T.-D. Kim, J.-W. Kang, J. Luo, S.H. Jang, J.W. Ka, N. Tucker, J.B. Benedict, L.R. Dalton, T. Gray, R.M. Overney, D.H. Park, W.N. Herman, A.K.-Y. Jen, Journal of the American Chemical Society 129 (2007) 488.
[27] K. Miyairi, E. Itoh, Proceedings of the International Conference on Solid Dielectrics, 2004.
[28] M. Hochberg, T. Baehr-Jones, G. Wang, J. Huang, P. Sullivan, L. Dalton, A. Scherer, Optics Express 15 (2007) 8401.
[29] Y. Song, J. Wang, Q. Li, M. Yan, M. Qiu, Optics Express 18 (2010) 13173.
[30] N.S. Lagali, M.R. Paiam, R.I. MacDonald, IEEE Photonics Technology Letters 11 (1999) 665.
[31] J.G. Grote, J.S. Zetts, R.L. Nelson, F.K. Hopkins, L.R. Dalton, C. Zhang, W.H. Steier, Optical Engineering 40 (2001) 2464.
[32] K. Sekine, Colloid and Polymer Sciences 264 (1986) 943.
[33] F. Mousty, P. Ostoja, L. Passari, Journal of Applied Physics 45 (1974) 4576.